JOURNAL OF CATALYSIS 137, 36–50 (1992)

The Interaction of Vanadia with Sepiolite. Structural Studies by ^{51}V Solid-State NMR and Raman Spectroscopy

MARIO L. OCCELLI,* ROBERT S. MAXWELL,† AND HELLMUT ECKERT†

*Georgia Tech Research Institute, Georgia Institute of Technology, Materials Science and Technology Laboratory, Atlanta, Georgia 30332; and †Department of Chemistry, University of California, Santa Barbara, Goleta, California 93106

Received December 6, 1991; revised March 9, 1992

The interaction of vanadium with sepiolite, a layered magnesium silicate used to stabilize cracking catalysts against metal contaminants in crude oils, is investigated. To this end, field-dependent ^{51}V wideline, magic-angle-spinning (MAS), and nutation NMR studies, together with X-ray diffraction (XRD) and laser Raman spectroscopy (LRS) results, are reported on sepiolite samples impregnated with a solution of vanadyl napthenate in benzene. These results are discussed in connection with benchmark NMR data of crystallographically well-defined model compounds in the $MgO–V_2O_5$ system. When heated near 760°C in the presence of steam, sepiolite decomposes into enstatite ($MgSiO_3$) and silica. If the hydrothermal treatment is repeated in the presence of vanadium, a disordered microcrystalline phase of α-$Mg_2V_2O_7$ forms. Steam treatment at higher temperatures results in the formation of β-$Mg_2V_2O_7$. In addition, all samples examined contain an amorphous surface phase. Based on ^{51}V nutation NMR spectroscopy, this amorphous constituent is inferred to have a structural environment similar to β-$Mg_2V_2O_7$. An MgV_2O_6-like, distorted octahedral environment is present only in samples with very high surface coverages and can be suppressed by choosing multiple-step over single-step impregnation.

INTRODUCTION

The difficulty of converting more abundant, less expensive, nickel- and vanadium-contaminated residuum feedstocks and crude oils into liquid products by fluid catalytic cracking is well recognized (*1*). Previous research has shown that the deleterious effects of metal contaminants such as Ni and V on fluidized cracking catalysts' (FCC) performance can be drastically reduced by the addition of materials, such as sepiolite, that can irreversibly and selectively sorb vanadium (and nickel) in the form of heat stable metal compounds (*2–4*). The V-passivating properties of the aforementioned materials have been attributed to the formation of microcrystalline magnesium vanadates (*3*) or to the formation of amorphous two-dimensional vanadium(V) oxide overlayers of the type observed on certain metal oxides (*5–8*).

In a typical commercial cracking unit, the catalyst is continuously regenerated by removing occluded hydrocarbons and coke deposits using hydrothermal and thermal treatments. The effects of regeneration on catalyst properties are simulated in the laboratory by exposing experimental catalysts to steam at high temperature (760–815°C) for a short period of time (5–10 h). Thus, the first step toward an understanding of vanadia–scavenger interactions has been the spectroscopic investigation of model systems that reflect these conditions. Such systems have been prepared by impregnation of sepiolite with solutions of vanadyl naphthenate in benzene, followed by calcination and hydrothermal treatment with 100% steam at 1 atm at 760°C for 5 h (*2–4*).

Due to the poor crystallinity of the samples involved, the characterization methods required to study vanadium–surface interactions are those that can provide information on local environments rather than on long-range structural order. As previously

0021-9517/92 $5.00

demonstrated, solid-state ^{51}V NMR is an element-selective, often inherently quantitative technique with considerable potential in this regard (*6–15*). Past applications of this technique have focused on the structural environment of amorphous vanadium(V) compounds on metal oxide supports. Recently, ^{51}V NMR also has been used to monitor the destruction of FCC components by vanadium contaminants (*16*). In the present contribution, ^{51}V NMR is used to investigate the interaction of sepiolite with vanadium in samples containing different V loadings prepared using different processing conditions. These studies will be complemented by NMR and laser Raman investigations on binary compounds in the $MgO–V_2O_5$ system.

EXPERIMENTAL

Sepiolite. The sample of Spanish Sepiolite (from TOLSA, S.A., nominal formula $Mg_4Si_6O_{15}(OH)_2$) used in the present study has been found to contain a clay mineral characterized by a typical fibrous structure, high surface area (142 m^2/g), and high pore volume (0.68 cc/g). The composition was verified by wet chemical analysis; calculated composition: SiO_2, 66.8 wt%; MgO, 29.9 wt%; found: SiO_2, 64.4 wt%; MgO, 27.8 wt%; Al_2O_3, 1.4 wt%; Fe_2O_3, 0.41 wt%; CaO, 0.14 wt%; Na_2O, 0.10 wt%. This clay was essentially free from phase impurities and gave an X-ray pattern in excellent agreement with JCPDS (Joint Committee on Powder Diffraction Standards) pattern No. 13-595 for sepiolite. After steaming (760°C/5 h), the clay retained 70% of its original BET surface area and its pore volume remained essentially unchanged.

Vanadium loading. A solution of vanadyl naphthenate (Pfaltz and Bauer) in benzene was used to metal load the fresh catalysts according to an established procedure (*17*). Decomposition of the naphthenate was performed by heating for 10 h at 540°C in air. The V-loaded clay samples were then steam-aged for 5 h with ~100% steam at 760°C in a fluidized bed. In a separate set of experiments, the steaming temperature was varied between 760 and 815°C for a sample impregnated with 5 wt% V using multiple steps. Analyses carried out on representative samples confirmed that batch compositions are generally close (within 0.1 wt%) to the actual vanadium content. All samples were characterized by BET surface area measurements as well as by X-ray powder diffraction (Siemens D-500 diffractometer) at a scan rate of 1°/min using monochromatic Cu$K\alpha$ radiation.

Model compounds. Reference vanadates were prepared by first pressing MgO/V_2O_5 mixtures at 10,000 lb/in^2 and then heating the resulting wafers in air in the 600–1200°C temperature range (*3*). By varying MgO/V_2O_5 ratios and calcination temperatures it was possible to obtain MgV_2O_6, α-$Mg_2V_2O_7$, β-$Mg_2V_2O_7$, and $Mg_3V_2O_8$ crystals essentially free from major phase impurities. Further details of the preparation of these compounds have been given elsewhere (*3*).

Raman spectroscopy. Raman spectra were recorded on a Spex Ramalog 1403 spectrometer equipped with a cooled RCA GaAs photomultiplier tube (CA 31034-02). The 4880-Å line of an argon-ion laser (Spectra Physics model 165) was used to generate Raman scattered light. The laser power impinging on the sample was limited to 50 mW. All spectra were recorded with a spectral resolution of 5 cm^{-1}. Signal pulses from the photomultiplier were passed through an amplifier/discriminator (Princeton Applied Research model 1182) and counted by a Nicolet data system. Typically, 50 scans were averaged in order to obtain spectra with good signal-to-noise ratios. Samples were prepared for Raman measurements by pressing the V-loaded sepiolite into 1-cm diameter wafers with a pressure of approximately 1000 psi. The sample holder rotated at approximately 500 rpm in order to avoid temperature-induced chemical modifications of the sample by the incident laser beam (*3*).

Nuclear magnetic resonance. Solid-state ^{51}V NMR studies were undertaken at 79.0

and 131.48 MHz, using General Electric GN-300 and GN-500 spectrometers with probes from Doty Scientific. Wideline NMR spectra were typically obtained at 79.0 MHz with a simple one-pulse sequence (Bloch decay), using 10° pulses of 1 μs length, a preacquisition delay of 10 μs, dwell time of 1–2 μs, and relaxation delays of 1 s. Although the use of Bloch decays bears the potential danger of resulting in somewhat distorted lineshapes, it is the preferred method here since it avoids complications arising from varying degrees of excitation selectivity that become important with the longer pulse lengths needed to generate 90° and 180° pulses for spin echoes (*9*). Magic-angle-spinning (MAS) NMR spectra were obtained both at 79.0 and 131.48 MHz, using variable spinning speeds ranging from 5 to 9 kHz and chemical shifts are referenced relative to $VOCl_3$. ^{51}V nutation NMR studies were undertaken at a rotary frequency of 27.8 kHz, corresponding to a liquid 90° pulse of 9 μs. In addition, most of the samples were characterized by ^{29}Si MAS-NMR, which was carried out at 59.7 MHz, with a 90° pulse of 8 μs length, and with relaxation delays of 2–4 min.

RESULTS, DATA ANALYSIS, AND INTERPRETATION

The experiments described in this section address three topics related to the action of sepiolite as a cracking catalyst stabilizer: (1) the decomposition of sepiolite upon thermal treatment and steam-aging as studied by X-ray and ^{29}Si MAS-NMR; (2) the interaction of sepiolite and its decomposition products with vanadia, as studied by surface area and ^{51}V NMR measurements; and (3) the structural characterization of the vanadium environments in the resulting products, interpreted in conjunction with solid-state NMR and Raman spectroscopic studies of vanadate model compounds.

Thermal decomposition of sepiolite. Figure 1 shows X-ray powder diffraction patterns of representative samples investigated. Even in the presence of V impurities, sepiolite exhibits excellent thermal stability and after calcination at 540°C/10 h in air retains most of its initial crystallinity, pore volume, and surface area.

When heated at 760°C/5 h in the presence of steam at 1 atm, this clay collapses, forming a poorly crystallized orthorhombic $MgSiO_3$ (enstatite) phase; see Fig. 1b. Furthermore, some silica is probably present; the diffraction lines at $\theta = 20°–22°$ in Figs. 1c–1d are consistent with the presence of poorly crystallized tridymite. (These peaks are not observed in all of the samples, however.) If the steam-aging temperature is increased to 788 or 815°C, enstatite crystallinity improves significantly; see Figs. 1c and 1d. When heated near 800°C in air, sepiolite decomposes into enstatite and quartz (*3*). However, for samples heated between 760 and 815°C in the presence of steam, our X-ray patterns give no evidence for quartz formation. (see Figs. 1b and 1d).

Figure 2 shows ^{29}Si MAS-NMR spectra of representative samples. The parent sepiolite shows three sharp ^{29}Si resonances at -92, -95, and -98 ppm corresponding to the three crystallographically distinct sites in the structure (*18, 19*). As found in previous studies (*19*), however, substantial broadening of the ^{29}Si NMR resonances occurs upon calcination to 540°C. This finding can be attributed to the presence of variable, slightly distorted local environments. There is also some signal intensity in the $Q^{(4)}$ region, suggesting that also a small amount of condensation (under loss of hydroxyl units) has occurred.

In excellent agreement with X-ray diffraction data, the ^{29}Si MAS-NMR results reveal that the steam-treatment at 760°C results in the decomposition of sepiolite into enstatite and silica. ^{29}Si MAS-NMR is particularly useful to monitor this decomposition, since ^{29}Si chemical shifts show unique ranges for the various types of SiO_4 tetrahedra that exist in minerals. These tetrahedral units are labeled $Q^{(n)}$, where n refers to the number of bridging (as opposed to nonbridging) oxygen atoms per silicon (*20*). The sepiolite decomposition,

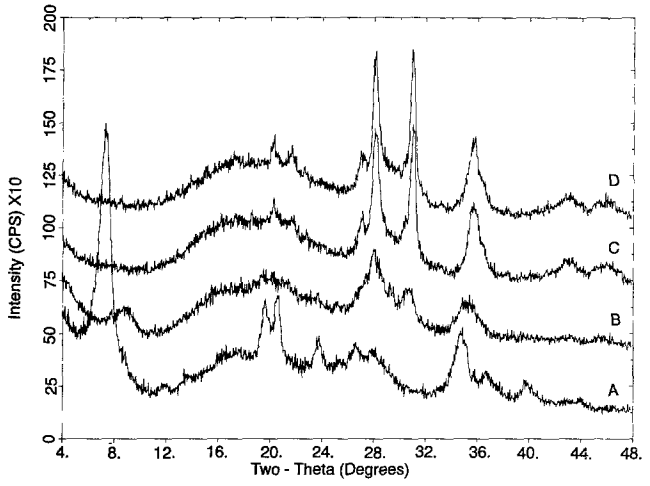

FIG. 1. X-ray powder diffraction patterns of sepiolite after loading with 5 wt% V and (A) calcination in air for 10 h at 540°C, followed by steam-aging for 5 h at (B) 760°C, (C) 788°C, and (D) 815°C.

$$Mg_4Si_6O_{15}(OH)_2 \rightarrow 4\ MgSiO_3 + 2\ SiO_2 + H_2O, \quad (1)$$

corresponds to a disproportionation of $Q^{(n)}$ species according to the scheme

$$2\ Q^{(3)} \rightarrow Q^{(2)} + Q^{(4)}. \quad (2)$$

Accordingly, Fig. 2 shows that separate ^{29}Si MAS-NMR peaks are resolvable for enstatite ($Q^{(2)}$, -83 ppm), sepiolite ($Q^{(3)}$, peak center at -97 ppm for the heated samples), and silica ($Q^{(4)}$, -110 ppm). As are the X-ray diffraction patterns, the MAS-NMR spectra are broadened substantially, indicating strong disordering effects in these product phases. Investigation of a large number of samples with different V loadings reveals that the extent of the decomposition at 760°C is somewhat variable, but generally greater in samples with higher V loadings. The use of steam-aging temperatures higher than 760°C results in complete sepiolite decomposition according to Eq. (1); see Figs. 1, 2a).

In contrast to X-ray data, the ^{29}Si MAS-NMR spectra clearly reveal the presence of the silica phase. The peak position is certainly compatible with the tridymite resonance. However, in contrast to the published NMR spectrum of tridymite (*21*), no separate peaks for crystallographically inequivalent silicon sites are resolvable.

Vanadia–sepiolite interaction. Figure 3 shows the effect of the vanadia–sepiolite interaction upon the surface areas for one set of samples, prior to and after steam-

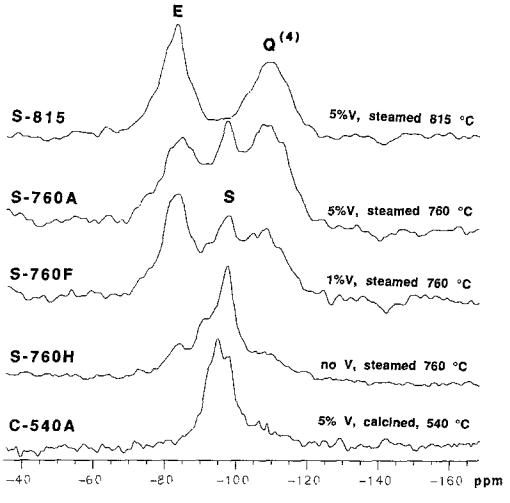

FIG. 2. ^{29}Si MAS-NMR spectra of representative spectra. The phases, enstatite and sepiolite, are abbreviated by their initials. The $Q^{(4)}$ resonance due to disordered silica is also indicated.

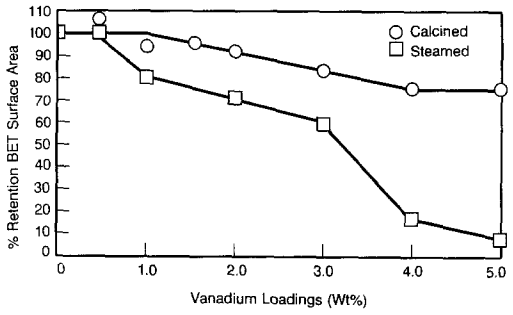

FIG. 3. The effect of vanadia on the surface area of sepiolite: After V impregnation and thermal, or hydrothermal, treatment.

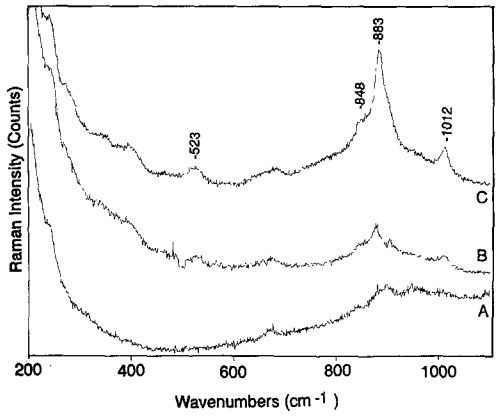

FIG. 4. Raman spectra of sepiolite after loading with 5 wt% V and calcination in air for 10 h at 540°C, followed by steam-aging for 5 h at (A) 760°C, (B) 788°C, and (C) 815°C.

aging, as a function of vanadium loading. Evidently, conversion of vanadyl naphthenate to a vanadium (V) surface oxide phase by calcination at 540°C has only a modest effect on the sepiolite surface area, whereas steam-aging at 760°C can result in a collapse of the surface. The surface collapse at V loadings above 3%, particularly after steam-aging, suggests the formation of bulk phases.

Although X-ray diffraction and ^{29}Si MAS-NMR are useful to follow the decomposition of the sepiolite upon steam-aging, they cannot provide information on the nature of the reaction products resulting from vanadium–sepiolite interaction. In contrast, techniques such as ^{51}V NMR and laser Raman spectroscopy can identify the formation of V compounds even when poorly crystalline and when present in low concentrations. Laser Raman spectroscopy results for steam-aged, V-loaded sepiolite samples have indicated that above 3 wt% V, new broad and weak peaks begin to appear. In addition, samples containing 5 wt% V, when steam-aged at 760°C, generate a spectrum containing broad and weak bands centered at 846, 903, and 950 cm^{-1}, consistent with the presence of α-$Mg_2V_2O_7$; see Figs. 4a and 5b. At higher steaming temperatures, new bands develop near 1012, 883, and 523 cm^{-1}, generating a spectrum similar to that of β-$Mg_2V_2O_7$ (*3*); see Figs. 4 and 5. The relatively broad bands in Fig. 4 are attributed to a highly dispersed vanadate phase, in agreement with the NMR results.

Figures 6a–d show wideline ^{51}V NMR results as a function of vanadium loading and thermal treatment, respectively. Figures 7a–e summarize high-speed 79.0 MHz MAS-NMR data, their dependence on loading level, the effect of steam treatment, and the influence of the treatment temperature. Table 1 gives an overview of the samples studied and the assignments and conclu-

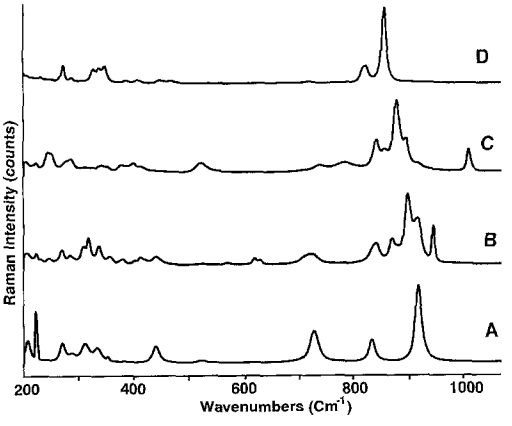

FIG. 5. Raman spectra of model binary magnesium vanadates: (A) MgV_2O_6; (B) α-$Mg_2V_2O_7$; (C) β-$Mg_2V_2O_7$; (D) $Mg_3V_2O_8$.

TABLE 1

Preparation History, Vanadium Contents, and Surface Areas (θ) of the Samples under Study and the Phases Identified by ^{51}V NMR

Code and sample information		wt%V	$\theta(m^2/g)$	Phases present
	Sepiolite samples, calcined at 540°C, 10 h			
C-540A	single impregnation	5	105	V(4) + α,β-$Mg_2V_2O_7$
C-540B	single impregnation	4	110	not detd.
C-540C	single impregnation	3	123	V(4)
C-540D	single impregnation	2	144	not detd.
C-540E	single impregnation	1.5	147	not detd.
C-540F	single impregnation	1	143	not detd.
C-540G	single impregnation	0.5	142	not detd.
C-540H	single impregnation	0	150	
C-540	multiple impregnation	5		V(4) + α,β-$Mg_2V_2O_7$
	Sepiolite samples, calcined at 540° (10 h) and steamed at 760°C (5 h)			
S-760A	single impregnation	5	9	V(4) + V(6)
S-760AA	2-step impregnation	5	17	V(4) + α-$Mg_2V_2O_7$
S-760B	single impregnation	4	20	V(4) + V(6)
S-760BB	2-step impregnation	4	27	V(4) + tr. V(6)
S-760C	single impregnation	3	60	V(4) + tr. V(6)
S-760CC	2-stp impregnation	3	40	V(4) + tr. V(6)
S-760D	single impregnation	2	69	V(4)
S-760DD	single impregnation	2	44	V(4)
S-760E	single impregnation	1.5	not detd.	V(4)
S-760EE	single impregnation	1.5	43	V(4)
S-760F	single impregnation	1	76	V(4)
S-760FF	single impregnation	1	56	V(4)
S-760G	single impregnation	0.5	95	not detd.
S-760GG	single impregnation	0.5	57	V(4)
S-760H	no impregnation	0	97	
S-760HH	no impregnation	0	64	
S-760	multiple impregnation	5	34	V(4) + α-$Mg_2V_2O_7$
S-788	multiple impregnation	5		V(4) + α,β-$Mg_2V_2O_7$
S-815	multiple impregnation	5		V(4) + β-$Mg_2V_2O_7$

Note. Sample codes refer to the figures.

sions based on the model compound work discussed below.

Model compound studies. As mentioned in the Introduction, the formation of bulk crystalline or amorphous compounds in the $MgO–V_2O_5$ system is believed to play a role in the stabilizing activity of sepiolite. The $MgO–V_2O_5$ phase diagram has been the subject of considerably detailed study (*22*). Four crystalline binary phases are known whose stoichiometries are $Mg_3(VO_4)_2$, $Mg_2V_2O_7$ (two polymorphs, α (LT)- and β (HT)-phase, with a reported transition temperature range of 710–760°C depending on heating conditions), and MgV_2O_6. The local environments of the V atoms in these phases, well known from X-ray crystallography, are summarized in Fig. 8 (*22–26*). Preliminary ^{51}V NMR results on magnesium vanadates have been published by Mastikhin and co-workers (*13*). However, these authors did not carry out the field-dependent NMR experiments necessary to separate the effects of second-order quadrupolar couplings and chemical shift effects on the MAS-NMR spectra. As previously discussed for other quadrupolar nuclei (*7*), the experimentally measured resonance positions comprise the isotropic

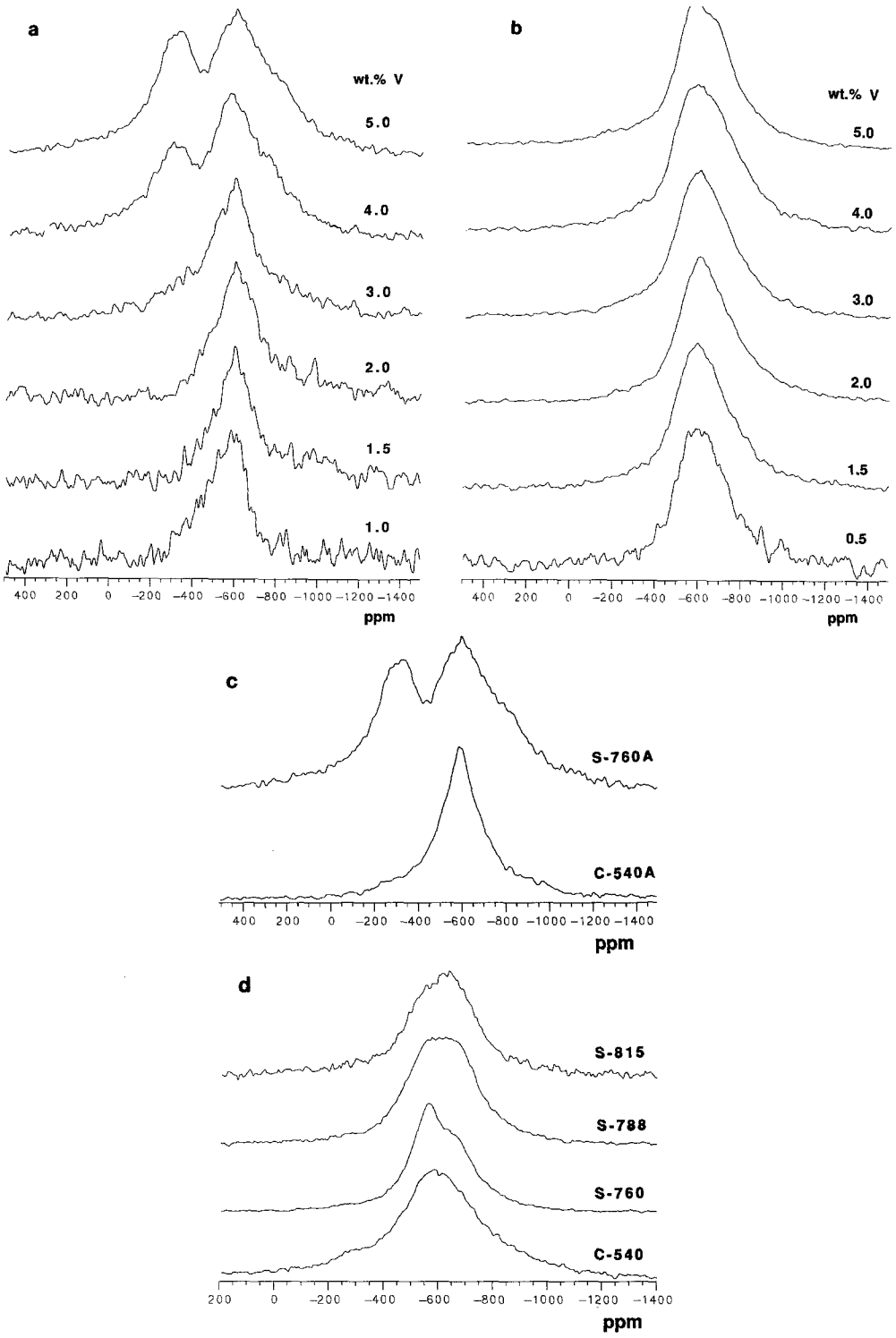

FIG. 6. (a) 79.0 MHz ^{51}V wideline NMR spectra of vanadium(V) oxides on sepiolite, as a function of concentration (wt% V). These samples were prepared in a single loading step with vanadium naphthenate. (b) 79.0 MHz ^{51}V wideline NMR spectra of vanadium(V) oxides on sepiolite, as a function of concentration (wt% V). Samples containing more than 3 wt% V were prepared in multiple loading steps with vanadium naphthenate. (c) 79.0 MHz ^{51}V wideline NMR spectrum of sepiolite–5% V, prior to and after steam-aging. (d) 79.0 MHz ^{51}V wideline NMR spectra of sepiolite–5% V, steam-aged at different temperatures.

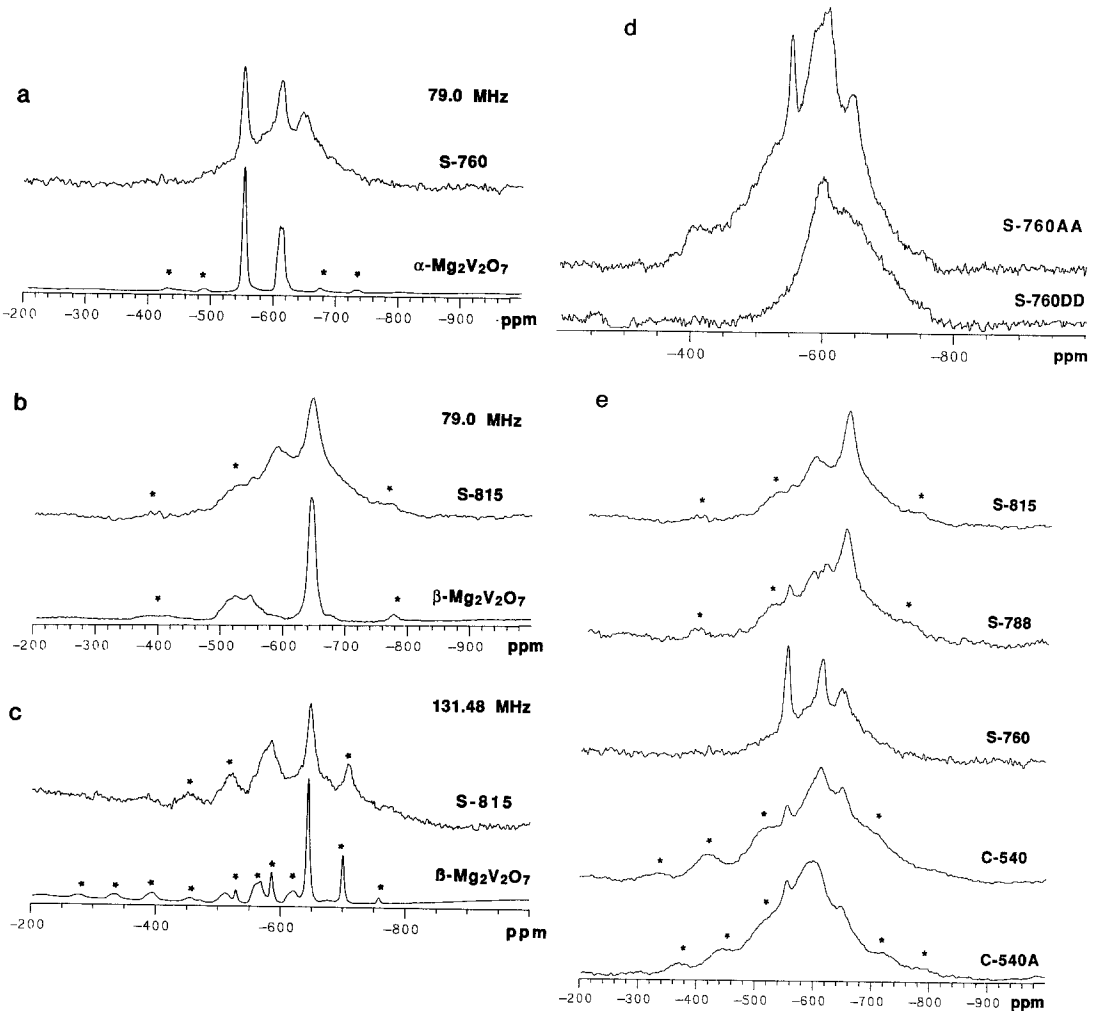

FIG. 7. (a) Comparison of the 79.0 MHz ^{51}V MAS-NMR spectra for sample S-760 and α-$Mg_2V_2O_7$, substantiating peak assignments. (b) Comparison of the 79.0 MHz ^{51}V MAS-NMR spectra for sample S-815 and β-$Mg_2V_2O_7$, substantiating peak assignments. Spinning sidebands are indicated by asterisks. (c) Comparison of the 131.48 MHz ^{51}V MAS-NMR spectra for sample S-815 and β-$Mg_2V_2O_7$, substantiating peak assignments. (d) Comparison of the 79.0 MHz ^{51}V MAS-NMR spectra for samples S-760DD and S-760AA, illustrating the effect of vanadium loading. (e) 79.0 MHz ^{51}V MAS-NMR spectra of calcined and steam-aged 5% V-sepiolite samples, illustrating the influence of thermal treatment conditions.

chemical shift δ_{iso} and the second-order quadrupolar shift $\delta^{(2)}$:

$$\delta_{exp} = \delta_{iso} + \delta^{(2)}. \quad (3a)$$

For a spin-7/2 nucleus such as ^{51}V, the magnitude of $\delta^{(2)}$ is given by

$$\delta^{(2)}\,[\text{ppm}] = -2551\nu_o^{-2}(e^2qQ/h)^2(1 + \eta^2/3), \quad (3b)$$

where ν_o is the nuclear Larmor precession frequency in Hz and e^2qQ/h and η are the nuclear electric quadrupole coupling constant (in Hz) and the asymmetry parameter, respectively.

Representative static ("wideline") and MAS-NMR spectra for these model compounds are shown in Figs. 9 and 10. The wideline NMR lineshapes are dominated by

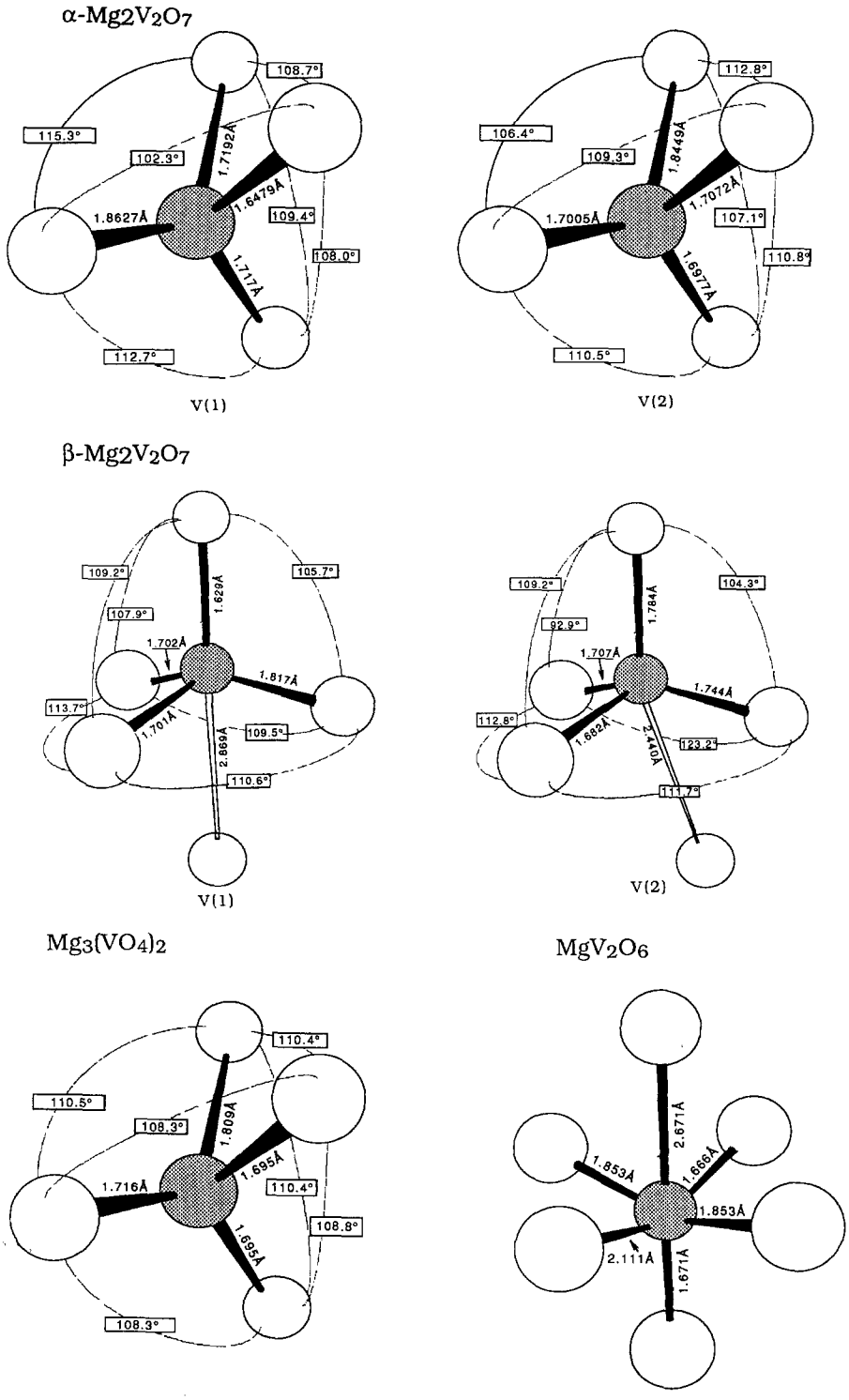

FIG. 8. Structural environments present in crystalline magnesium vanadates.

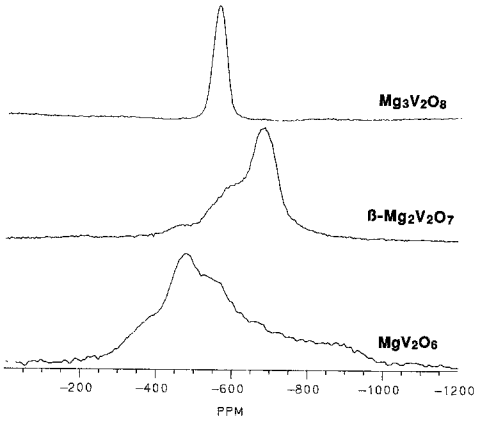

FIG. 9. 79.0 MHz wideline (static) ^{51}V NMR spectra of binary magnesium vanadates.

the chemical shift anisotropy. Upon MAS, these lineshapes yield spinning sideband patterns from which δ_{exp} as well as approximate values for the principal tensor components δ_{ii} can be extracted. Table 2 summarizes this information, including the δ_{iso} values determined by Eqs. (3) from the 79.0- and 131.5-MHz measurements. To determine approximate values for δ_{ii}, the spinning sideband intensities measured at 131.48 MHz were analyzed by the graphical procedure of Herzfeld and Berger (*27*), followed by refinement using an interactive graphic simulation routine. Furthermore, Table 2 lists values of e^2qQ/h and η as determined from computer-simulations of the 79.0 MHz MAS-NMR central lineshapes (*28*). Since this analysis is possible only for those compounds that have peak shapes with resolvable second-order structure, data for several compounds are not shown. The quadrupolar coupling parameters extracted in this fashion are compared with some low-field single-crystal NMR data (in parentheses) where available (*29, 30*). For all of the compounds studied, the second-order quadrupolar shifts at 11.7 T calculated with Eq. (3b) from field-dependent MAS experiments were consistent with the quadrupolar parameters determined by fitting the shape of MAS-NMR centerbands.

Figure 11 shows ^{51}V nutation NMR studies of vanadia–sepiolite samples and binary magnesium vanadate model compounds. These experiments probe the strength of the nuclear electric quadrupole interaction by measuring the length of the effective 90° pulse. In principle, the NMR spectrum for ^{51}V in solids consists of seven allowed $m \rightarrow m - 1$ Zeeman transitions. For very weak quadrupolar interactions, all of these transitions are effectively excited. In this case one measures a 90° pulse length close to that seen in liquid solutions. If, on the other hand, the quadrupole interaction is strong compared to the strength of the applied rf field, only the central $1/2 \rightarrow -1/2$ transition is excited. Due to first-order quadrupolar perturbation, all of the other transitions are spread out over a wide frequency range that lies mostly outside of the excitation window of the rf pulse. It was previously shown that in such a situation the effective 90° pulse length is shortened significantly, the limit being $t_{90}^{liquid}/4$ for a spin-7/2 nucleus (*31–33*). Thus, measurements of the effective 90° pulse length are useful to estimate the strength of the nuclear electric quadrupolar interaction, at least on a relative basis. Displayed in Fig. 11 are stacked plots of normalized Fourier transforms at 0.5-μs pulse increments. The effective 90° pulse lengths (required to reach the maximum signal) are listed as a separate entry in Table 2.

DISCUSSION

In the following, we first discuss the NMR results of the model compounds, shown in Figs. 9–11, in the context of the known structural features of the $MgO–V_2O_5$ system. This information then serves to advance the interpretation of the NMR data on the vanadia–sepiolite samples, shown in Figs. 6 and 7.

$MgO–V_2O_5$ model compounds. $Mg_3V_2O_8$ crystallizes in the space group *Cmca;* the asymmetric unit contains one isolated VO_4^{3-} unit (*23*). Applying the $Q^{(n)}$ nomencla-

TABLE 2

^{51}V NMR Parameters for the V(V) Sites Present in Crystalline Magnesium Vanadates and for the Disordered V(V) Sites in the Sepiolite Samples

Sample	$\delta_{79.0}$[a] (ppm)	$\delta_{131.48}$[a] (ppm)	δ_{11}[b] (ppm)	δ_{22}[b] (ppm)	δ_{33}[b] (ppm)	δ_{iso} (ppm)	e^2qQ/h (MHz)	η[d]	t_p (μs)
$Mg_3V_2O_8$	−554	−554	csa too small to determine			−554	≤1(0.49)	(0.63)	5.5
α-$Mg_2V_2O_7$									
site 2	−554	−552	−599	−561	−495	−551			
site 1	−614	−608	−704	−591	−532	−605	4.6	0.55	
β-$Mg_2V_2O_7$									
site 2[c]	−535	−511	−669	−602	−262	−497	9.5(10.2)	0.70(0.42)	
site 1	−648	−644	−724	−670	−539	−642	(4.7)	(0.26)	3.2
MgV_2O_6	−562	−553	−890	−444	−353	−548	[e]	[e]	2.6
V(4)	−590 ± 2	−580 ± 2	not determined			−574			3.5
V(6)	not measured		−280 ± 20	−300			not determined		

Note. $\delta_{79.0}$ and $\delta_{131.48}$ (typical errors ± 1 ppm) correspond to the resonance locations at 79.0 and 131.48 MHz, respectively. δ_{11}, δ_{22}, and δ_{33} (estimated error ± 5 ppm) are the principal tensor components determined graphically from the MAS-sideband patterns observed at 131.48 MHz. δ_{iso}, the isotropic chemical shift (±2 ppm) has been calculated from $\delta_{79.0}$ and $\delta_{131.48}$. For suitable cases, values for e^2qQ/h and η were obtained from simulations of the MAS centerbands recorded at 79.0 MHz.

[a] ±1 ppm.

[b] ±5 ppm unless specified.

[c] Error in δ_{ii} values ±10 ppm.

[d] Errors in e^2qQ/h and η are 0.1 MHz and 0.02, respectively. Where no data are reported, the quadrupole coupling is too weak to affect the central MAS lineshape.

[e] MAS lineshape analysis not possible due to signal overlap from impurity of α-$Mg_2V_2O_7$.

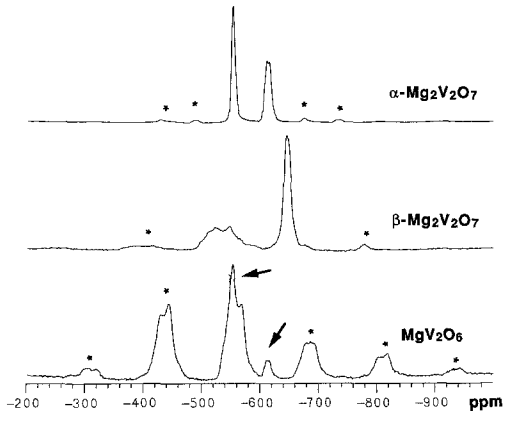

FIG. 10. 79.0 MHz ^{51}V MAS-NMR spectra of binary magnesium vanadates. Spinning sidebands are indicated by asterisks. In the spectrum of MgV_2O_6, minor impurity peaks due to α-$Mg_2V_2O_7$ are marked by arrows.

ture (n specifying the number of bridging oxygen atoms) to the vandium sites, this is a $Q^{(0)}$ site, the four nonbridging oxygen atoms forming a weakly distorted tetrahedral environment. The V–O bond lengths range from 1.695 to 1.809 Å, and all the angles are close to tetrahedral. This comparatively high degree of symmetry results in a chemical shift anisotropy that is so small that it is noticeable neither in the wideline spectra (see Fig. 9a) nor in any spinning sideband patterns generated by MAS (spectrum not shown). Furthermore, the nuclear electric quadrupole interaction is so weak that under the experimental conditions employed in this study the second-order quadrupolar shift is zero within experimental error (1 ppm). Figure 11 reveals that the effective 90° pulse length is shortened only moderately in comparison to that measured in the liquid, revealing that the rf excitation of the ^{51}V resonance is partially nonselective.

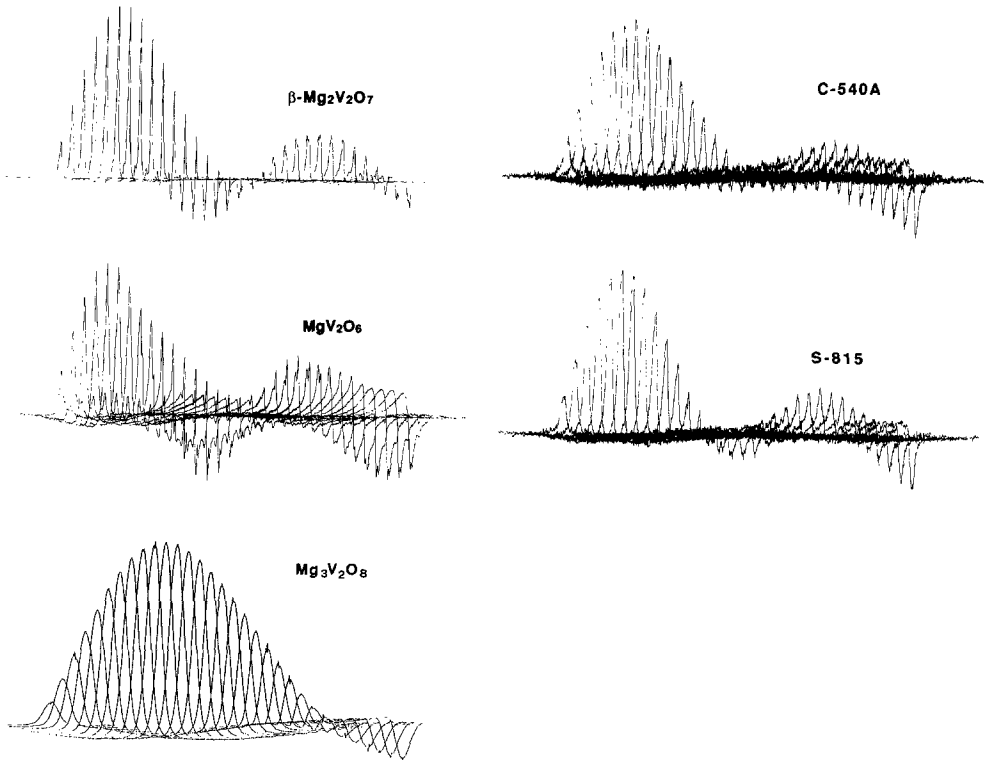

FIG. 11. ^{51}V nutation NMR behavior of vanadium(V) oxide on sepiolite samples containing 5 wt% V (samples C-540 and S-815) and comparison with crystalline model compounds.

The crystal structure of low-temperature α-$Mg_2V_2O_7$ has not yet been solved by single-crystal X-ray diffraction. Since powder X-ray data indicate that this compound is isomorphous with $Co_2V_2O_7$ (space group $P2_1/c$), the vanadium environments in these two compounds are taken to be identical (*24*). This structure is characterized by $[O_3V–O–VO_3]^{4-}$ dimers, with both crystallographically inequivalent vanadium atoms in distorted tetrahedral $Q^{(1)}$ environments. The MAS-NMR spectrum shows two distinct resonances, with marked differences in second-order quadrupole shifts. Based on the information given in Fig. 8, we assign the resonance at $\delta_{iso} = -551$ ppm to the less distorted vanadium (2) site, because this peak has the smaller second-order quadrupolar shift.

The high-temperature modification, β-$Mg_2V_2O_7$, crystallizes in the triclinic space group $P\bar{1}$. Its structure is also based on $V_2O_7^{4-}$ dimers ($Q^{(1)}$ units), however, with fifth oxygen neighbors in close proximity (2.44 and 2.87 Å, at V(2) and V(1), respectively). The MAS-NMR spectrum shows two resonances, one of which ($\delta_{iso} \sim -497$ ppm) is characterized by an unusually strong nuclear electric quadrupolar interaction (*25*). Based on the observation of very strong ^{27}Al quadrupole couplings for five-coordinated aluminum environments (*34*), we assign this resonance to the V(2)-site. The ^{51}V principal shielding tensor components of this site are markedly different from those seen for either four- or six-coordinated vanadium sites, hence confirming that the description of this compound as being five-coordinate is realistic. Since due to strong second-order broadening, the 7.05 T

wideline spectrum of the V(2) site is not observed, the nutation behavior shown in Fig. 11 reflects the behavior of the V(1) site only.

MgV_2O_6 crystallizes in the monoclinic space group $C2/m$. The vanadium atoms are in an irregular six-coordinate environment, with V–O bond distances between 1.666 and 2.671 Å (*26*). The structure resembles those of a variety of other metavanadates of divalent metal cations. All of these compounds have a unique and diagnostic NMR signature, characterized by a large, close to axially symmetric chemical shift anisotropy and strong nuclear electric quadrupole coupling (*7*). The latter manifests itself in a large second-order quadrupolar shift, a structured ^{51}V MAS center band, and rf excitation behavior that is essentially restricted to the central transition. Overall, the different structural environments depicted in Fig. 8 give rise to distinct and unique behavior in the various NMR experiments discussed here. Thus, the model compounds provide useful benchmark data for discussion of the details of the vanadia–sepiolite interactions.

Vanadia–sepiolite interaction. Figures 6a–d show representative ^{51}V wideline NMR spectra of calcined and steam-aged sepiolite samples loaded with vanadia. In general, fairly broad and unstructured lineshapes are observed, bearing little resemblance to the spectra observed for bulk binary magnesium vanadates. However, this should not be taken as evidence against the formation of microcrystalline magnesium vanadates. In fact, these lineshapes could have been altered by distribution effects in chemical shifts or quadrupole coupling parameters and by the presence of paramagnetic electron spins. The spectra of samples with lower loadings (%V $\leq$ 3) and, concomitantly, lower surface coverages, are characterized by a signal centered near -600 ppm. In conjunction with previous model compound studies (*7*), this resonance is assigned to four-coordinate vanadium(V), most likely of type $Q^{(1)}$. At higher loadings (%V $\geq$ 4) a new resonance gradually emerges on the downfield side of the spectrum. Earlier studies have shown that this second signal can be attributed to a near-to axial chemical shift powder pattern centered around -500 ppm (*7*). The nearly degenerate perpendicular components of this shift tensor are located near -300 ppm and the parallel component between -800 and -900 ppm (*7*). These parameters are in proximity to those observed in MgV_2O_6, where vanadium possesses a distorted six-coordinated environment. Previous NMR studies on vanadium(V) oxide surface phases and model compounds have shown that such a spectroscopic signature is unique and characteristic for a vanadium(V) species in a distorted octahedral environment (*6, 7*).

Figure 6c illustrates that the six-coordinated environment appears only after steam-aging, presumably following the collapse of the sepiolite surface. Apparently, it takes very high surface coverages (several monolayers) to establish this environment on the sepiolite surface, and its formation can be minimized at 5 wt% V altogether by multiple deposition (i.e., by depositing the precursor in several separate steps, see Fig. 6b). The behavior of vanadia on sepiolite contrasts sharply with the results obtained with vanadia on alumina, titania, and silica surfaces, where the octahedral site can be found already at submonolayer coverages (*6, 7, 9*). Figure 6d shows subtle wideline NMR lineshape changes in the 5 wt% V sample prepared by multiple impregnation and steam-aged at temperatures above 760°C. This behavior is related to the formation of different bulk magnesium vanadates, which becomes more fully evident in the MAS-NMR data discussed below.

Besides providing a rough distinction between four- and six-coordinate vanadium environments, ^{51}V wideline NMR spectra are not capable of resolving further details. Figures 7a–e show ^{51}V MAS-NMR spectra at spinning speeds between 8 and 9 kHz for a variety of samples. Several of these spectra show distinct sharp MAS-NMR center bands and sideband patterns, from which the pres-

ence of both α- and β-$Mg_2V_2O_7$ is evident. Note that the ^{51}V peaks assignable to these phases are somewhat broadened, reflecting residual disorder or small crystallite sizes of these magnesium vanadates. (This may well be the reason for the inability to observe these compounds by X-ray powder diffraction.) Figures 7a,b show that the relative ratio of the α- and β-phases depends on the temperature of the steam treatment and the observed behavior is found to be consistent with the stability regions of both polymorphs (*22*). Thus, in the sample steam-aged at 760°C, α-$Mg_2V_2O_7$ is more abundant, whereas the β-phase dominates at the higher steaming temperatures (788 and 815°C). Figure 7c illustrates the improvement in resolution that can be achieved at a higher field strength (11.7 vs 7.0 T). The identification of β-$Mg_2V_2O_7$ in these vanadia–sepiolite samples is largely based on the observation of the V(1) site and the dependence of its spectrum on field strength. The spectra show no clear evidence for the highly distorted V(2) site. We believe this to be a consequence of the residual disorder of the $Mg_2V_2O_7$ formed. The spectrum of the V(2) site, which is already difficult to detect in the bulk crystalline state (resonance near -510 ppm in Fig. 7c, bottom), is particularly sensitive to this disorder, and probably broadened beyond detectability due to a distribution of $\delta^{(2)}$ values. In addition to the resonances due the bulk magnesium vanadates, Figures 7a–c also show a broad resonance around -590 ppm (-580 ppm at 131.48 MHz, plus associated spinning sidebands), which is attributed to an amorphous surface phase.

Figure 7d shows that bulk magnesium vanadates are not detectable in steam-aged samples with lower vanadium loadings (2 wt% V). Only a broad signal, with a distinct feature around -590 ppm (at 7.05T) is seen, suggesting that all of the vanadium is contained in amorphous surface phases.

Finally, Fig. 7e compares the spectra of the steam-aged samples with those of their calcined precursors. In the calcined samples, only traces of defined binary phases can be discerned and their 79.0 MHz MAS-NMR spectra are dominated by the broad resonance centered near -590 ppm. As mentioned above, this resonance also persists in the steam-aged samples, particularly at low loadings (Figs. 7a–d), suggesting that in addition to the microcrystalline pyrovanadate phases there is a different, somewhat less well ordered, type of vanadium environment. An estimate of δ_{iso} for this site is given in Table 1. The assignment of this line is less straightforward. Both the wideline spectra and the nutation behavior clearly rule out a six-coordinated environment. At the same time, the wideline spectra are found to be significantly broader than those obtained for vanadium(V) surface oxide on MgO samples (*13, 35*), which have been generally assigned to VO_4^{3-} $Q^{(0)}$ groups. Altogether, the spectroscopic parameters and the nutation behavior are most consistent with an assignment to a dimeric $V_2O_7^{4-}$ group. If this assignment is accepted, the NMR data suggest that the basic molecular $V_2O_7^{4-}$ architecture on the sepiolite surface is already in place prior to steam-aging, presumably in the form of a disordered surface phase. The role of the steaming process then mainly appears to be to convert the disordered arrangement of these units into microcrystalline $Mg_2V_2O_7$ phases. Overall, the ^{51}V MAS-NMR results are well in agreement with LRS data that have suggested the formation of $Mg_2V_2O_7$ phases when V-loaded sepiolite granules are exposed to steam at temperatures in the 700–800°C range (*3*) (see Fig. 4).

CONCLUSIONS

In summary, the results shown here confirm the suitability of ^{51}V wideline, MAS, and nutation NMR to provide information about local vanadium environments and bulk phases formed during the course of the interaction of vanadia with sepiolite. In the present system, such information is not accessible by X-ray powder diffraction. The ^{51}V MAS-NMR data, together with LRS

data, confirm that the interaction of vanadia with sepiolite produces both amorphous phases, as well as bulk α- and β-$Mg_2V_2O_7$, depending on temperature. The formation of these bulk phases is favored by sample steaming and high vanadia loadings, which also favor the decomposition of the parent sepiolite into silica and enstatite. In fact, the suitability of sepiolite for vanadium passivation may be intimately linked to its decomposition, as the structural breakdown facilitates the reaction of Mg with vanadia species on a molecular scale.

ACKNOWLEDGMENTS

This research was partially supported by NSF Grant DMR-89-13738 (to H.E.). MLO is particularly grateful for the support received from the Unocal Analytical Department. Special thanks are due to Dr. P. Ritz, P. Iyer, and M. Bell for providing Raman and XRD data and for many useful discussions. This research was supported by NSF Grant DMR-89-13738 to HE.

REFERENCES

1. Occelli, M. L., *in* "Fluid Catalytic Cracking: Role in Modern Refining" (M. L. Occelli, Ed.), p. 1. ACS Symposium Series, Vol. 375, ACS, Washington, DC, 1988.
2. Occelli, M. L., *in* "Fluid Catalytic Cracking: Role in Modern Refining" (M. L. Occelli, Ed.), p. 162. ACS Symposium Series, Vol. 375, ACS, Washington, DC, 1988.
3. Occelli, M. L., and Stencel, J. M., *in* "Fluid Catalytic Cracking: Role in Modern Refining" (M. L. Occelli, Ed.), p. 125. ACS Symposium Series, Vol. 375, ACS, Washington, DC, 1988.
4. Occelli, M. L., and Stencel, J. M., *in* "Zeolites as Catalysts, Sorbents and Detergent Builders" (Y. E. Karge and J. Weitkamp, Eds.), p. 127. Elsevier, Amsterdam, 1989.
5. Haber, *J. Pure Appl. Chem.* **56,** 1663 (1984).
6. Eckert, H., and Wachs, I. E., *Mater. Res. Soc. Symp. Proc.* **111,** 455 (1988).
7. Eckert, H., and Wachs, I. E., *J. Phys. Chem.* **93,** 6796 (1989).
8. Occelli, M. L., and Stencel, J. M., *in* "Fluid Catalytic Cracking II: Concepts in Catalyst Design" (M. L. Occelli, Ed.), p. 252. ACS Symposium Series, Vol. 452, ACS, Washington, DC, 1991.
9. Le Costumer, L. R., Taouk, B., Le Meur, M., Payen, E., Guelton, M., and Grimblot, J., *J. Phys. Chem.* **92,** 1230 (1988).
10. Taouk, B., Guelton, H., Grimblot, J., and Bonnelle, J. P., *J. Phys. Chem.* **92,** 6700 (1988).
11. Chary, K. V. R., Rao, V. V., and Mastikhin, V. M., *J. Chem. Soc. Chem. Commun.*, 202, (1989).
12. Eckert, H., Deo, G., Wachs, I. E., and Hirt, A. M., *Colloids Surf.* **45,** 347 (1990).
13. Lapina, O. B., Simakov, A. V., Mastikhin, V. M., Veniaminow, S. A., and Shubin, A. A., *J. Mol. Catal.* **50,** 55 (1989).
14. Rigutto, M. S., and Van Bekkum, H., *Appl. Catal.* **68,** L1 (1991).
15. Hardcastle, F. D., Wachs, I. E., Eckert, H., and Jefferson, D. A., *J. Solid State Chem.* **90,** 194 (1991).
16. Iyer, P., Eckert, H., Occelli, M. L., and Stencel, J. M., *in* "ACS Symposium Series," Vol. 452, p. 242. ACS, Washington, DC, 1991.
17. Mitchell, B. R., *Ind. Eng. Chem. Prod. Res. Dev.* **19,** 209 (1980).
18. Komarneni, S., Fyfe, C. A., and Kennedy, G. J., *Clays Clay Miner.* **34,** 99 (1986).
19. Barron, P. F., and Frost, R. L., *Am. Mineral.* **70,** 758 (1985).
20. Lippmaa, E., Mägi, M., Samoson, A., Engelhardt, G., and Grimmer, A. R., *J. Am. Chem. Soc.* **102,** 4889 (1980).
21. Pettifer, R. F., Dupree, R., Farnan, I., and Sternberg, U., *J. Non-Cryst. Solids* **106,** 408 (1988).
22. Clark, G. M., and Morley, R. *J. Solid State Chem.* **16,** 429 (1976), and references therein.
23. Ng, H. N., and Calvo, C., *Can. J. Chem.* **50,** 3619 (1972).
24. Sauerbrei, E. E., Faggiani, R., and Calvo, C., *Acta Crystallogr., Sect. B* **30,** 2907 (1974).
25. Krishnamachari, K., and Calvo, C., *Can. J. Chem.* **49,** 1629 (1971).
26. Gopal, R., and Calvo, C., *Acta Crystallogr. Sect. B* **30,** 2491 (1974).
27. Herzfeld, J., and Berger, A. E., *J. Chem. Phys.* **73,** 6021 (1980).
28. Samoson, A., Kundla, E., and Lippmaa, E., *J. Magn. Reson.* **49,** 350 (1982).
29. Andronenko, I. V., Dmitrieva, L. V., Molodchenko, N. G., Moskalev, V. V., and Zonn, Z. N., *Sov. Phys. Solid State (Engl. Transl.)* **21,** 535 (1979).
30. Gubanov, V. A., Lasukova, N. N., and Pletnev, R. N., *Zh. Neorg. Khim.* **23,** 655 (1978).
31. Samoson, A., and Lippmaa, E., *Phys. Rev. B.* **28,** 6567 (1983).
32. Kentgens, A. P. M., Lemmens, J. J. M., Geurts, F. M. M., and Veeman, W. S., *J. Magn. Reson.* **71,** 62 (1987).
33. Man, P. P., Theveneau, H., and Papon, P., *J. Magn. Reson.* **64,** 271 (1985).
34. Alemany, L., and Kirker, G., *J. Am. Chem. Soc.* **108,** 6158 (1986).
35. Eckert, H., and Wachs, I. E., to be published.